Synthetic Metals 160 (2010) 468–474

Contents lists available at ScienceDirect

Synthetic Metals

journal homepage: www.elsevier.com/locate/synmet

Synthesis, characterization and comparative OFET behaviour of indenofluorene–bithiophene and terthiophene alternating copolymers

Prashant Sonar[a], Luke Oldridge[a], Andrew C. Grimsdale[a,1], Klaus Müllen[a,*], Mathieu Surin[b], Roberto Lazzaroni[b], Philippe Leclère[b], Jason Pinto[c], Lay-Lay Chua[c], Henning Sirringhaus[c], Richard H. Friend[c]

[a] Max-Planck-Institute für Polymerforschung, Ackermannweg 10, D-55128 Mainz, Germany
[b] Université de Mons, Place du Parc 20, B-7000 Mons, Belgium
[c] Cavendish Laboratory, University of Cambridge, Madingley Road, Cambridge CB3 0HE, United Kingdom

ARTICLE INFO

Article history:
Received 5 August 2009
Received in revised form 27 October 2009
Accepted 24 November 2009
Available online 24 December 2009

Keywords:
Indenofluorene copolymers
Semiconducting Materials
Microscopic Morphology
Charge
Carrier Mobility

ABSTRACT

The synthesis of alternating copolymers of tetraalkylindenofluorene with bithiophene and terthiophene using Suzuki polycondensation route is reported. We report on the optical and electrochemical properties of these copolymers. AFM analysis of the microscopic morphology of thin deposits showed that the copolymer with terthiophene units produced the more ordered films, with well-defined fibrillar structures, resulting from highly-regular dense packing due to strong π–π interchain interactions, in contrast to the amorphous bithiophene copolymer. Upon testing these materials in FETs the terthienyl copolymers displayed the higher charge mobilities among the studied compounds, with values of over 10^{-4} cm^2 V^{-1} s^{-1} being obtained.

1. Introduction

Organic thin film field effect transistors (OFETs) using both oligomeric and polymeric materials have received attention because of their potential applications such as low cost large area flexible displays and low end data storage such as smart cards [1–5]. Organic materials possess the advantages of easy processing (e.g. spin-coating, printing, evaporation), good compatibility with a variety of substrates including flexible plastics, and considerable scope for tuning of their properties by structural modification. Over the past few years, an extensive range of functionalized π-conjugated materials have been designed and synthesized with desirable optoelectronic properties. Electron donor (hole transporting) and electron acceptor (electron transporting) materials with thermal/chemical stability, solution processability, charge carrier mobility, and controllable HOMO–LUMO energy levels are essential for these applications.

Among these materials, well-defined thiophene oligomers have been intensively studied, because of their relatively high charge carrier mobilities [4]. A potential problem with thiophene-based materials is that due to their high-lying highest occupied molecular orbitals (HOMO), they are readily oxidized (e.g. by environmental oxygen) which reduces the efficiencies and lifetimes of devices. One way to reduce this problem is to introduce other moieties with lower lying HOMOs, such as tetraalkylindenofluorenes [5]. Indenofluorene-based homopolymers and copolymers are widely used in OLED research, but as far as we know, there are no reports of using these materials for OFET applications.

In this paper, we report the synthesis of alternating copolymers of tetraoctylindenofluorene with oligothiophenes containing two and three thiophene units, and a study of the effects of varying the size of the oligothiophene moieties on their microscopic morphology and optoelectronic properties, including their performance in FETs. We demonstrate how the difference in OFET behaviour is intrinsic to their structural differences.

2. Experimental

2.1. Materials

All commercially available materials were used as received unless otherwise noted. All reactions were carried out using

* Corresponding author.
E-mail address: muellen@mpip-mainz.mpg.de (K. Müllen).
[1] [1]Current address: School of Materials Science and Engineering, Nanyang Technological University, 50 Nanyang Avenue, Singapore 639798, Singapore.

0379-6779/$ – see front matter.
doi:10.1016/j.synthmet.2009.11.033

Schlenk techniques under an argon or nitrogen atmosphere in anhydrous solvents.

2.2. Characterization

^{1}H and ^{13}C NMR spectra were recorded on a Brucker Avance 250 MHz spectrometer using tetramethylsilane as an internal standard. Infrared spectra were measured as oils or as KBr pellet using a PerkinElmer spectrometer. Gel Permeation Chromatography (GPC) analysis against polystyrene or polyphenylene [6] standards was performed in THF on a Waters high pressure GPC assembly with an M590 pump, μ-Styragel columns of 10^5, 10^4, 10^3, 500 and 100 Å and a refractive index detector. UV–vis absorption spectra were obtained on a PerkinElmer Lambda 15 spectrophotometer. Photoluminescence spectra were recorded on a SPEX Fluorolog 2 Type F212 steady-state fluorimeter, using a 450 W xenon arc lamp as excitation source and a PMT R 508 photomultiplier as detector system. CV was performed on an EG&G Princeton Applied Research Potentiostat, Model 270 on 2 μm thick films deposited by solution coating onto pre-cleaned ITO as a working electrode with an area of 0.2 cm^2. After coating, the films were dried in a vacuum oven for 10 min. The measurements were carried out in acetonitrile solutions containing 0.1 M of tetrabutylammonium perchlorate as the supporting electrolyte, using Ag/AgCl as reference electrode and a platinum wire as counter electrode, respectively, and an internal ferrocene/ferrocenium (FOC) standard.

The copolymers were tested in two different FET configurations—bottom-gate bottom-contact and top gate. Bottom-gate bottom-contact transistors were prepared on highly doped n^{++} silicon with a thermally grown oxide layer approximately 2000 to 2200 Å thick. Source and drain electrodes were composed of an interdigitated 30 nm thick gold array with a 3 to 5 nm chromium adhesion layer. Prior to use the substrates were cleaned, oxygen plasma etched, and then exposed to hexamethyldisilazane (HMDS) vapour for several hours. The HMDS treatment rendered the SiO_2 surface hydrophobic. The polymer solutions in chloroform or xylene were spin cast onto the HMDS treated substrate after passing through a 0.2 μm filter. All spin casting was performed in the inert atmosphere of a nitrogen glove box and produced films approximately 90 nm thick. Samples were annealed at this stage on a hotplate inside the glove box. Top gate transistors were prepared on glass with gold-chromium arrays similar to the bottom-gate bottom-contact substrates. The substrates were cleaned and oxygen plasma etched before spin-casting the filtered polymer solutions. Once spin-cast the films were annealed on a hot plate for the required time in the glove box. A poly(methyl methacrylate) (PMMA) gate insulator was then spin cast directly onto the semiconductor after filtering and the top gate gold electrode evaporated onto the gate insulator thereby completing the transistor structure. Transistor characteristics were measured in a nitrogen glove box using an Agilent 4155C Semiconductor Parameter Analyzer.

2.3. Synthetic procedure

2.3.1. 2,8-Bis(4,4,5,5-tetramethyl-1,3,2-dioxaborolan-2-yl)-6-6′,12,12-tetraalkyl-6,12-dihydroindeno-(1,2b)-fluorene (2)

A solution of n-butyllithium in hexanes (2.53 mL, 2.5 M, 6.34 mmol) was added to a stirred solution of the dibromide **1** (2.60 g, 3.02 mmol) in dry THF (15 mL) at −78 °C. The mixture was stirred at −78 °C for 30 min., warmed to 0 °C for 15 min and then again cooled to −78 °C for 15 min. 2-Isopropoxy-4,4,5,5-tetramethyl-1,3,2-dioxaborolane (Aldrich) (1.32 g,7.10 mmol) was added rapidly to the solution and the resulting mixture was warmed to room temperature and stirred for 24 h. The mixture was poured into water and extracted with diethyl ether. The organic extracts were washed with brine and dried over magnesium sulphate. The solvent was removed by rotary evaporation and the residue was purified by column chromatography (silica, 10% ethyl acetate in hexane) to give the bisboronate **2** as a white solid (2.0 g, 69%). Found: C 80.47, H 10.49%; Calculated for $C_{64}H_{100}B_2O_4$: C 80.48, H 10.55%; δ_H (250 MHz, $CDCl_3$) 7.78–7.72(d, 4H, Ph), 7.70 (s, 4H, Ph), 2.02 (m, 8H, $4CH_2$), 1.38 (s, 24H, $8CH_3$), 1.25–1.09 (m, 40H, $20CH_2$), 0.78–0.59 (m, 20H, $4CH_2 + 4CH_3$), δ_C (62.5 MHz, $CDCl_3$) 151.05, 150.75, 144.81, 141.32, 133.85, 129.09, 119.09, 114.80, 84.06, 40.89, 32.16, 30.34, 29.62, 25.15, 24.15, 22.95,14.19.

FD–Mass Spectroscopy calcd for $C_{64}H_{100}$ B_2O_4: 955.13. Found: 955.0.

2.3.2. 5,5"-dibromo-[2,2';5',2"] terthiophene (4)

A solution of NBS (1.13 g, 6.4 mmol) in DMF (25 mL) was added drop wise to a solution of terthiophene (0.8 g, 3.2 mmol) with exclusion of light and the reaction mixture was stirred for 24 h, at room temperature with exclusion of light. The mixture was poured into water and extracted with diethyl ether. The organic extract was washed with brine and dried over magnesium sulfate. The solvent was removed under reduced pressure and the crude product was purified by column chromatography eluting with hexane to give the product **4** as a pale yellow solid. (1.2 g, 92%).

δ_H (250 MHz, $CDCl_3$) 7.18–6.98 (m, 4H, Th), 6.92–6.85 (d, 2H, Th); δ_C (62.5 MHz, $CDCl_3$) 138.50, 136.62, 133.86, 129.05, 122.89, 122.26, 109.66.

FD–Mass Spectroscopy calcd for $C_{30}H_{44}$: 406.18. Found: 406.0.

2.3.3. Poly(tetraoctyl-2,8-indenofluorene-co-bithiophene) (P1)

5,5′-Dibromobithiophene **3** (68 mg, 0.209 mmol), the diboronate **2** (0.2 g, 0.209 mmol), and $(PPh_3)_4Pd$ (0.034 mmol) were dissolved in a mixture of toluene (4 mL) and aqueous 2 M K_2CO_3 (2 mL). The solution was first put under a nitrogen atmosphere and then was refluxed with vigorous stirring for 72 h. The mixture was then poured into methanol (150 mL). The precipitate was recovered by filtration and washed with dilute HCl, then extracted for 24 h in a Soxhlet apparatus using acetone to remove oligomers and catalyst residues. Traces of catalyst were further removed by stirring with EDTA solution overnight. The crude polymer precipitate was twice dissolved in chloroform and reprecipitated from methanol to give **P1** as a gray powder (150 mg, 82%). Found: C 82.85, H 8.51, S 7.57%; Calculated for $(C_{60}H_{80}S_2)_n$: C 83.27, H 9.32, S 7.41%; δ_H (250 MHz, $CDCl_3$) 7.80–7.19 (br m, 12H, Ph-Th), 2.11 (m, 8H, $4CH_2$),1.70–0.5 (m, 60H, $24CH_2 + 4CH_3$); δ_C (62.5 MHz, $CDCl_3$) 152.52, 150.92, 149.74, 144.29, 140.71, 136.68, 132.84, 124.83, 123.98, 120.18, 114.46, 40.95, 32.19, 30.34, 29.63, 29.56, 22.97, 14.20.

2.3.4. Poly(tetraoctyl-2,8-indenofluorene-co-terthiophene) (P2)

5,5"-Dibromo-[2,2';5',2"] terthiophene **4** (43 mg, 0.104 mmol), the diboronate **2** (100 mg, 0.104 mmol), and $(PPh_3)_4Pd(0)$ (15 mg, 0.012 mmol) were dissolved in a mixture of toluene (6 mL) and aqueous 2 M K_2CO_3 (3 mL). The solution was first put under a nitrogen atmosphere and then was refluxed with vigorous stirring for 72 h. The mixture was then poured into methanol (150 mL). The precipitated material was recovered by filtration and washed with dilute HCl, then extracted for 24 h in a Soxhlet apparatus using acetone. Traces of catalyst were then removed from polymer by stirring with EDTA solution overnight. The crude polymer precipitate was twice dissolved in chloroform and reprecipitated from methanol to give **P2** as a red-brown powder (80 mg, 81%). Found: C 80.10, H 8.25, S 9.86%; Calculated for $(C_{64}H_{82}S_3)_n$: C 81.13, H 8.72, S 10.15%; δ_H (250 MHz, $CDCl_3$) 7.80–7.10 (br m, 14H, Th-Ph), 2.02 (br s, 8H, $4CH_2$), 1.70–0.50 (br m, 60H, $24CH_2 + 4CH_3$); δ_C (62.5 MHz, $CDCl_3$) 151.49, 150.08, 143.63, 141.02, 140.18, 135.73, 135.31, 132,20, 131.52, 130.98, 130.94, 127.86, 127.67, 124.18,

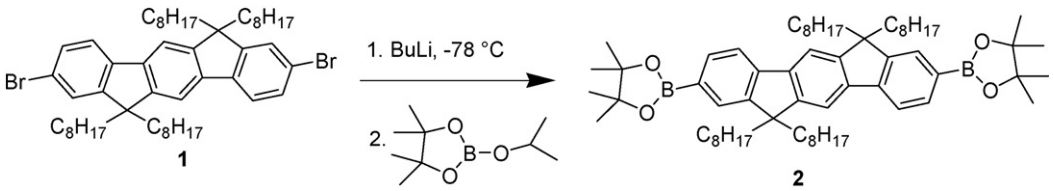

Scheme 1. Synthesis of monomer.

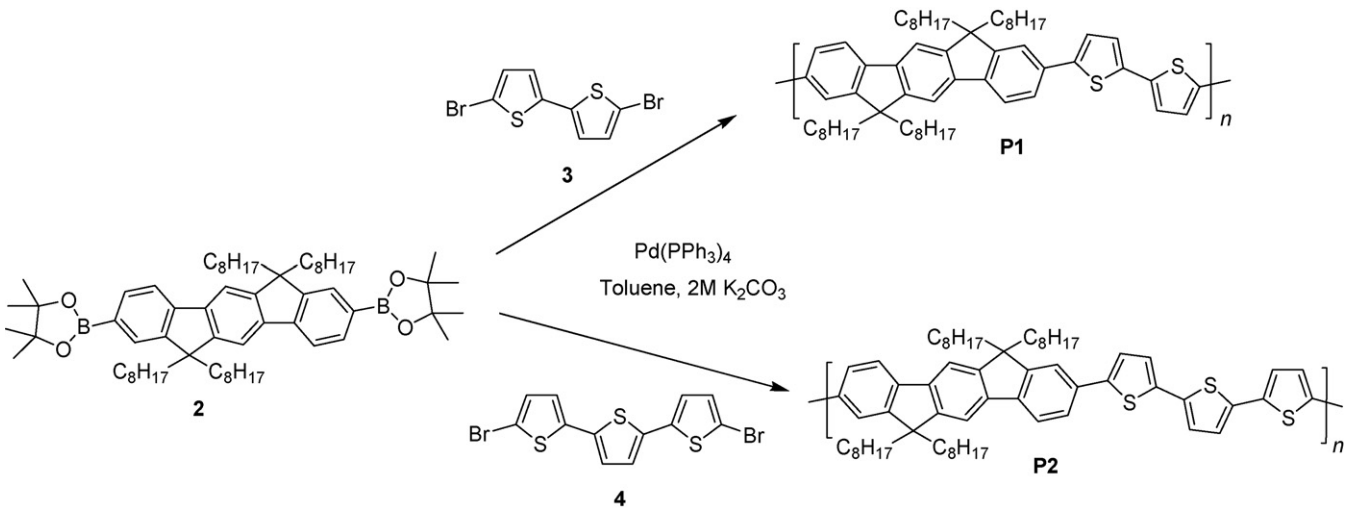

Scheme 2. Synthesis of polymer P1 and P2.

123.79, 123.34, 119.68, 119.00, 113.58, 54.42, 40.09, 31.41, 29.57, 28.82, 24.58, 23.62, 22.09, 13.04.

3. Results and discussion

3.1. Synthesis

Suzuki polycondensation route was utilized to prepare indenofluorene–bithiophene and terthiophene copolymers (**P1** and **P2**), respectively. The bisboronate of indenofluorene **(2)** was prepared from dibromoindenofluorene **(1)** according to a published procedure [7] (Scheme 1). Condensation of the bisboronate **2** with 2,2′-dibromobithiophene (**3**) produced polymer **P1** (PIF-T2) with moderate molecular mass (M_n = 20,000 g/mol, D = 4.64). In order to investigate the effect of longer oligothiophene units we next prepared the polymer **P2** (PIF-T3) by coupling 2,2″-dibromoterthiophene (**4**) with **2** (Scheme 2) under the same conditions as for preparation of **P1** above. This polymer was obtained with a similar molar mass (M_n = 19,900 g/mol, D = 4.50,) but unlike **P1** this polymer precipitated from the reaction medium. The molecular masses determined from GPC against polyphenylene standards [6] were found to be lower than from analysis against polystyrene standards. As the copolymers more closely resemble the rigid rod polyphenylenes, these lower values are probably more accurate, but the values against polystyrene are also given in Table 1 for comparison with literature values for similar polymers.

Both the copolymers possess high thermal stability with less than 5% loss being observed in thermogravimeric analysis below 400 °C, with the primary mass loss occurring at 400–450 °C. No liquid crystalline phases were detected by differential scanning calorimetry (DSC) or polarizing microscopy up to 300 °C. This is in contrast to the fluorene–bithiophene copolymer F8T2 which displays a liquid crystalline transition at 265 °C. [8] However, as the indenofluorene homopolymer exhibits higher liquid crystalline transition temperatures (250 and 290 °C [5]) than the corresponding polyfluorene (160 °C [9]), it is to be expected that any liquid crystalline transition temperatures for the indenofluorene copolymers will be higher than for the corresponding fluorene copolymers. The consequence for FET applications is that it is not be possible to align films of these copolymers to increase the charge carrier mobility by heating to 300 °C and then quenching as has been done for F8T2 [10].

Table 1
Molecular weight data for copolymers **P1** and **P2**.

Polymer	M_n (PS) (Da)	M_w/M_n (PS)	M_n (PPP) (Da)	M_w/M_n (PPP)
P1	20,000	4.64	14,200	3.08
P2	19,900	4.50	13,800	3.10

3.2. Optical properties

The absorption and PL spectra of the copolymers measured in chloroform using 10^{-5} M solutions are shown in Fig. 1a and b, respectively. The copolymer with bithiophene units exhibits an absorption maximum at 456 nm whereas for the terthiophene copolymer it is at 460 nm. We attribute this difference of 4 nm to the more extended conjugation length of the terthiophene as compared to the bithiophene copolymer. Optical band gaps calculated for both copolymers P1 and P2 from absorption cut off are 2.38 and 2.10 eV, respectively. From this observation it is quite clear that increasing the length of the conjugated oilgothiophene block reduces the band gap of the polymers. Both the polymers exhibited green emission with PL maxima at 529 nm and 554 nm, respectively. The 25 nm red shift for polymer **P2** compared to **P1** is attributed to the more extended conjugation in terthiophene (see Table 2). These polymers also markedly red shifted as compared to the emission from polyindenofluorene (λ_{max} = 432 nm), reflecting a reduction in the band gap due to the incorporation of bithiophene and terthiophene units.

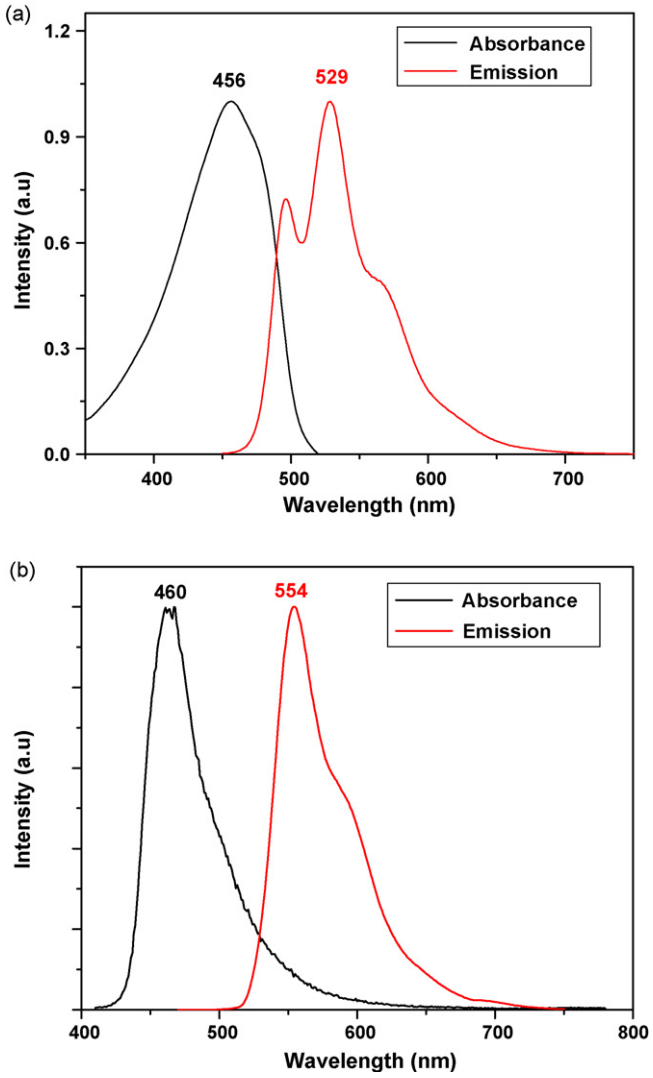

Fig. 1. Absorption and PL spectra for copolymer **P1** (a) and **P2** (b) in chloroform (10^{-5} M).

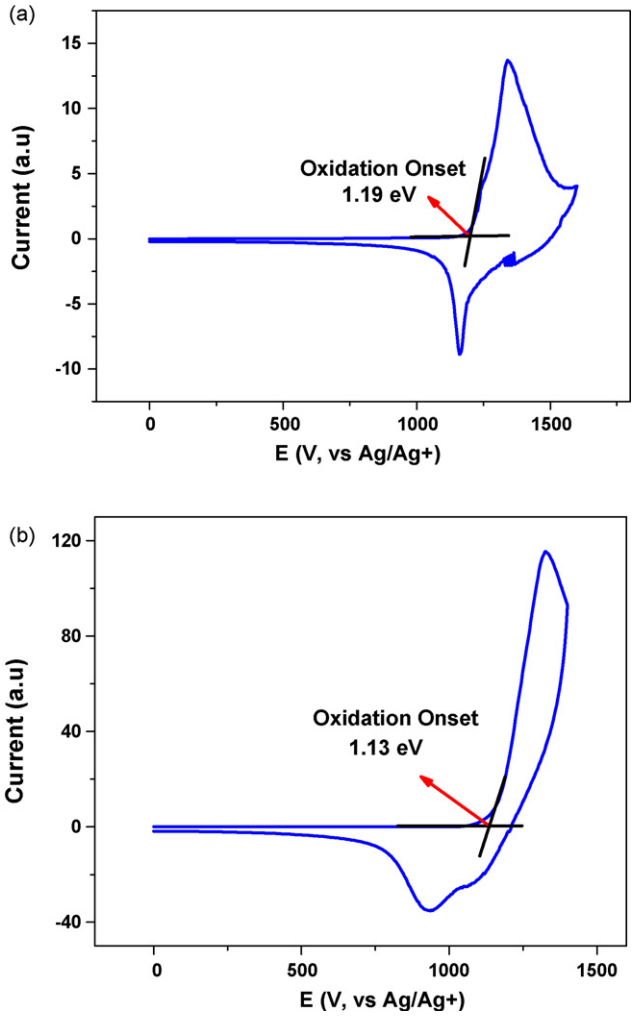

Fig. 2. Cyclic voltammogram for copolymers **P1** (a) and **P2** (b).

3.3. Electrochemical properties

The electrochemical properties were investigated in order to estimate the energy levels of the LUMO and HOMO of the polymers with respect to thiophene chain length and determine the electrochemical band gap. Cyclic voltammetry (CV) was performed against Ag/AgCl with an internal ferrocene/ferrocenium standard by the method of Janietz et al. [11] The onset potentials were determined from the intersection of two tangents drawn as the rising current and baseline charging current of the CV traces, and the HOMO energies calculated by using the known absolute energy of 4.4 eV for Ag/AgCl. The CV showed partially reversible oxidation in the range of 1.32–1.34 V, as compared to a value of 1.30 V recorded for pristine polythiophene [12] The cyclic voltammograms for **P1** and **P2** are shown in Fig. 2. Both copolymers showed a predominant partially reversible oxidation process but reduction process was not detected within the voltage range, which suggests the copolymers are better at hole than electron transporting. The oxidation onsets for bithiophene and terthiophene copolymers (**P1**) and (**P2**) were observed at 1.19 V and 1.13 V, respectively. As reduction was not observed, the LUMO energies were estimated by adding the optical band gap to the HOMO energies determined from CV. It should be noted that the optical band gap does not correspond to the electrical transport gap as these differ by an amount equal to the exciton binding energy, so that electrochemically measured LUMO values would differ from those here given. As the thiophene content increases in the copolymers the oxidation onset decreases as expected, indicating a rise in the HOMO level, but no effect on the LUMO energy levels was discernible (see Table 2). The HOMO level indicates that the material is oxidatively stable towards air—a key requirement for organic electronic devices.

Table 2
Optical and electrochemical data for copolymers **P1** and **P2**.

Polymer	Abs. λ_{max} (nm)	Band Gap (eV)[a]	PL λ_{max} (nm)	HOMO[b]	LUMO[c]
P1	456	2.38	529	5.59	3.21
P2	460	2.10	554	5.53	3.43

[a] Determined from absorption cut off.
[b] Calculated from oxidation onset against Ag/AgCl (4.4 eV).
[c] Estimated from HOMO value plus optical bandgap.

3.4. AFM analysis of the microscopic morphologies of the copolymers

We have recently shown that the microscopic morphology of thin deposits of conjugated materials (oligomers, polymers), as imaged with Tapping-mode Atomic Force Microscopy (TM-AFM), is a direct signature of the ability of the polymer chains to pack

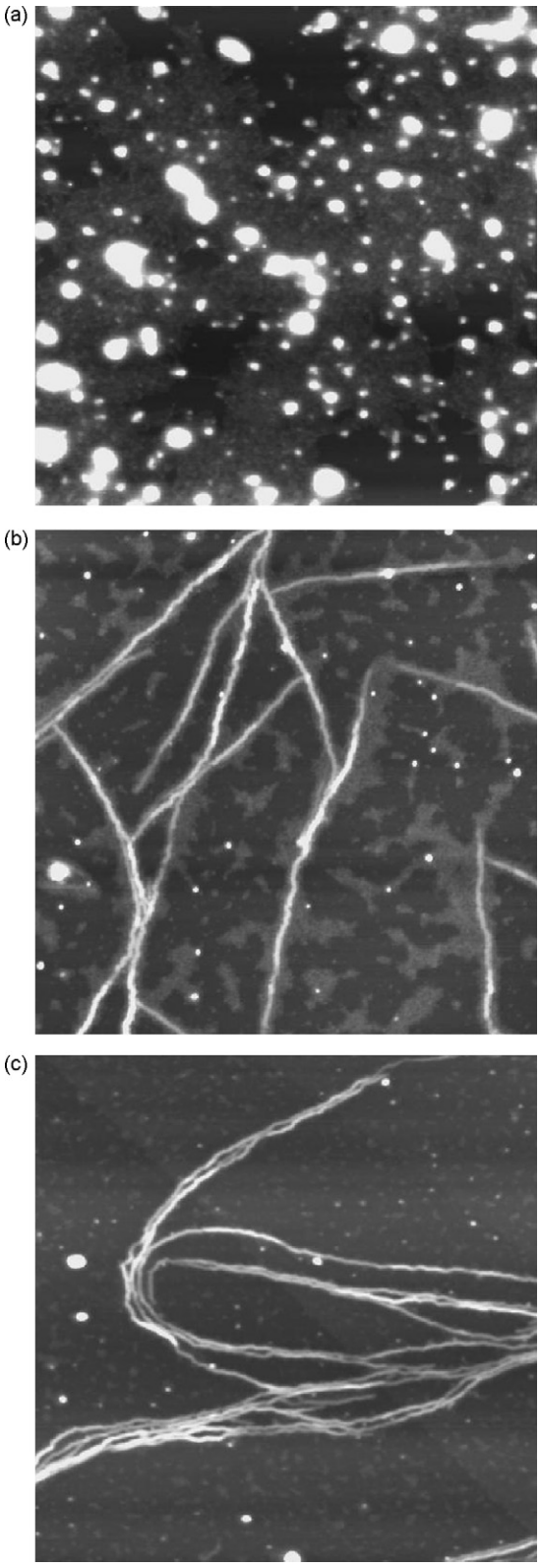

Fig. 3. TM-AFM height images (2.0 μm × 2.0 μm) of thin deposit from THF of **P1** on mica (top) and **P2** on mica (middle) and on graphite (bottom).

into compact, regular π-stacks [13–16]. Since the interchain interactions strongly impact on the charge transport properties, we investigated the microscopic morphology of thin deposits of the studied copolymers. Fig. 3a shows the microscopic morphology of a thin deposit of polymer **P1**. This image shows three levels of contrast non-organized aggregates that are a few tens of nm to a few hundreds of nm wide and few tens of nm high (bright objects), a monolayer/platelet (gray) and the mica substrate (dark). The average thickness of the monolayer is about 1.0 nm. Whatever the preparation conditions for the deposits, thin films of **P1** do not exhibit any ordered structure, but untextured aggregates of various sizes or μm-sized droplets (probably originating from dewetting).

However, thin deposits PIF-T3 (**P2**) clearly indicate a high degree of organization: in Fig. 3b and c respectively (Fig. 3a and b corresponds to deposits on mica and graphite, respectively); we clearly observe one-dimensional structures (in bright or gray) on the substrate (appearing dark). The fact that the same structures form on different substrates (mica: strongly hydrophilic; graphite: hydrophobic) is a sign that they originate from intrinsic self-assembly of the chains rather than specific interactions with the underlying substrate. These objects are a few hundreds of nm to μm-long, between 20 and 30 nm-wide, and a few nm-high (about 2–3 nm). This type of morphology is similar to the fibrillar structures ("nanoribbons") observed for example in deposits of homopolyfluorenes or homo-polyindenofluorenes [13,14]. In such structures, the organization originate from dense interchain packing due to π–π interactions: the molecules are parallel to each other, edge-on over the substrate with their stacking direction perpendicular to the stacking direction (i.e. the fibrillar axis), as supported by molecular modelling simulations [14,16,17]. Indeed, it has been shown that the commensurability between the length of the monomer units (indenofluorene is accommodated in front of a terthiophene, but not in front of a bithiophene) and the presence of alkyl groups are the two key structural factors governing the chain organization in alternated indenofluorene–oligothiophene copolymer assemblies [14]. From these results, it is clear that PIF-T3 (**P2**) exhibits highly ordered π-stacked structures while PIF-T2 (**P1**) leads to untextured aggregates

3.5. Electrical properties

Typical FET transfer characteristics for copolymer **P2** are shown in Fig. 4. Increasing drain current (I_d) with increasingly negative gate voltage implies p-type semiconductor activity as expected from the PIFs. A summary of measured device mobilities extracted from the transfer characteristics is listed in Table 3. Linear and saturated mobilities were calculated using Eqs. (1) and (2), respectively. The mobility was extracted from the largest slope of the square root of the transistor current in the saturation regime plotted as a function of gate voltage, while the threshold voltage was estimated from the intercept of the square root of the current in the saturation regime with the gate voltage axis

$$\mu_{lin} = \left.\frac{\partial I_d}{\partial V_g}\right|_{V_d=\text{const}} \frac{L}{WC_{\text{ins}}V_d} \quad (1)$$

$$\mu_{\text{sat}} = \left.\frac{\partial I_d}{\partial V_g}\right|_{V_d=\text{const}} \frac{L}{WC_{\text{ins}}\left(V_g - V_o\right)} \quad (2)$$

Significant hysteresis in the drain current could be observed when comparing the upward and downward voltage scans in both the transfer and output characteristics for most of these devices, which prevented the quantitative extraction of contact resistance values. This effect can be clearly observed in the output characteristics of a PIF-T3 device shown in Fig. 4. The hysteresis is probably caused by a decrease in drain current with time on the forward sweep followed by a recovery of the current at the start of the backward sweep. This non-ideality is an indication of a shifting turn on voltage during the measurement of the device, which is thought to be caused by slow charge trapping at the semiconductor–insulator interface or in the bulk of the semiconductor. This hypothesis was

Table 3
Mobility of copolymers from FET device characteristics (TG—top gate configuration, BG-BC—bottom-gate bottom-contact configuration).

Material		Linear Mobility ($cm^2\ V^{-1}\ s^{-1}$)		Saturated Mobility ($cm^2\ V^{-1}\ s^{-1}$)	
		BG-BC	TG	BG-BC	TG
PIF-T2	**P1**	1.9×10^{-5}, 2.5×10^{-5}, 125 °C anneal	3.5×10^{-6}	1.5×10^{-5}	4.6×10^{-6}
PIF-T3	**P2**	3.5×10^{-5}	3.5×10^{-6}, 200 °C anneal	$\mathbf{1.1 \times 10^{-4}}$	1.0×10^{-5}, 200 °C anneal

confirmed by varying the scan rate; the hysteresis was more pronounced at slower scan rates. Slow charge trapping occurs when charge carriers accumulated in the channel are captured at a trap site, as the measurement proceeds and then can no longer contribute to the drain current. On the backward scan, the charges then have time to become de-trapped and contribute to the drain current once the backward scan begins. The trap sites might be associated with chemical impurities in the semiconductor layer, either left over from the copolymer synthesis or introduced during device processing. Such chemical impurities might be particularly effective as charge traps in polymers of high ionization potential, such as the ones investigated here. To better evaluate the performance of **P2**, FETs were constructed using **P1** for comparison. Consistently, the FETs using **P2** showed mobilities nearly one order of magnitude higher than the corresponding devices using **P1** (FET data not shown in figure) fabricated by identical methods.

It is apparent from the mobility data that **P2** consistently showed a higher mobility than **P1** in all configurations tested. This is as expected from the structural characterization reported above. High temperature annealing (up to 200 °C for 5 min) improves the device stability somewhat and reduces the time-dependent instabilities without, however, significantly enhancing the measured mobility. The performance of **P2** was consistently one order of magnitude lower than for devices using the fluorene–bithiophene copolymer F8T2 with the same configuration and processing conditions. Further investigation of effects of annealing and more rigorous purification of the copolymers may produce further improvements in performance. No improvement in mobility, however, was seen from samples of **P2**, which had been subjected to rigorous purification including extensive washing with EDTA to remove metal residues. This suggests that the difference in mobility compared to F8T2 is intrinsic to the indenofluorene copolymer even though it has the same ratio of benzene and thiophene rings and similar packing to F8T2, indicating that there are more subtle factors involved in determining the absolute charge carrier mobilities in copolymers based on phenylene and thiophene units. Nonetheless the value of over $1 \times 10^{-4}\ cm^2\ V^{-1}\ s^{-1}$ obtained suggests that with further optimization **P2** may be suitable for device applications due to its excellent thermal stability.

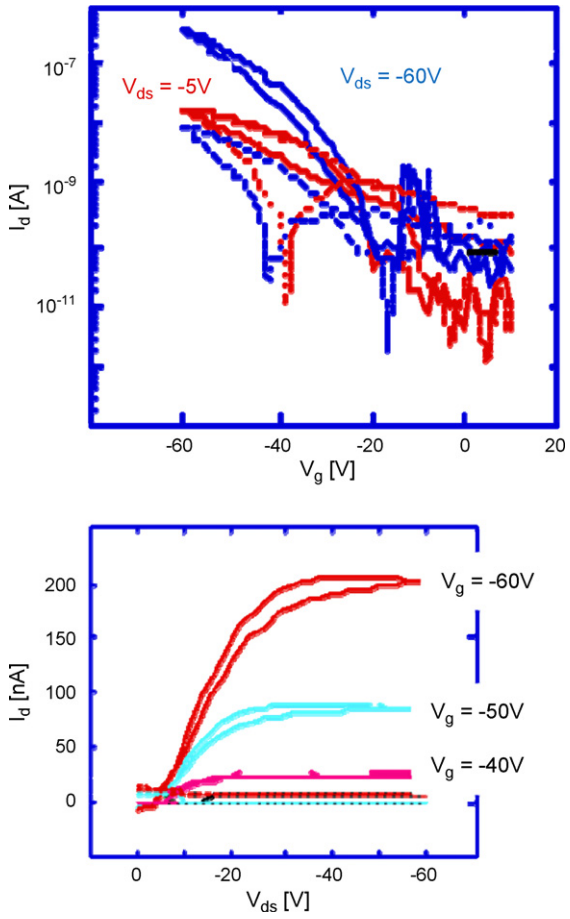

Fig. 4. Transfer and output device characteristics for P2 in bottom-gate bottom-contact configuration.

4. Conclusions

Copolymers of tetraoctylindenofluorene with bithiophene and terthiophene have been made and their optical and electronic properties studied. AFM analysis of their thin-film morphologies shows that the size of the oligothiophene units determines the chain packing. The terthiophene copolymer displays the highest degree of interchain order, with well-defined fibrillar morphology. The best mobility obtained was $1.1 \times 10^{-4}\ cm^2\ V^{-1}\ s^{-1}$, which suggests that these copolymers have promise as FET materials with further optimisation.

Acknowledgements

The authors are grateful to Christoph Sieber for electrochemical analysis, to Dr Jingying Zhang for measuring the fluorescence spectra, and to Jutta Schnee for technical assistance. The collaboration between Mons and Mainz is conducted within the framework of the Inter-University Attraction Pole Program (PAIV/3) of the Belgian Federal Government. Research in Mons is supported by the European Commission and the Government of the Région Wallonne (Phasing Out-Hainaut) and the Belgian National Fund for Scientific research FNRS/FRFC. Ph.L. and M.S. are Research Associates from the FRS-FNRS (Fonds National de la Recherche Scientifique, Belgium).

References

[1] G. Horowitz, Adv. Mater. 10 (1998) 365.
[2] Z. Bao, Organic and polymeric materials for thin film transistor applications, in: B. Hsieh, Y. Wei, M.E. Galvin (Eds.), Semiconducting Polymers, American Chemical Society, Washington, DC, 1999.
[3] F. Garnier, Acc. Chem. Res. 32 (1999) 209.
[4] H.E. Katz, Z. Bao, S. Gilat, Acc. Chem. Res. 34 (2001) 359.
[5] S. Setayesh, D. Marsitzky, K. Müllen, Macromolecules 33 (2000) 2016.
[6] S. Vanhee, R. Rulkens, U. Lehmann, C. Rosenauer, M. Schulze, W. Köhler, G. Wegner, Macromolecules 29 (1996) 5136.
[7] P. Sonar, J. Zhang, A. Grimsdale, K. Müllen, M. Surin, R. Lazzaroni, Ph. Leclère, S. Tierney, M. Henney, I. McCulloch, Macromolecules 37 (2004) 709.

[8] M. Grell, M. Redecker, K.S. Whitehead, D.D.C. Bradley, M. Inbasekaran, E.P. Woo, W. Wu, Liq. Cryst. 26 (1999) 1403.
[9] M. Grell, D.D.C. Bradley, M. Inbasekaran, Adv. Mater. 9 (1997) 798.
[10] H. Sirringhaus, R.J. Wilson, R.H. Friend, M. Inbasekaran, W. Wu, E.P. Woo, M. Grell, D.D.C. Bradley, Appl. Phys. Lett. 77 (2000) 406.
[11] S. Janietz, D.D.C. Bradley, M. Grell, C. Giebeler, M. Inbasekaran, E.P. Woo, Appl. Phys. Lett. 73 (1998) 2453.
[12] H.S.O. Chan, S.C. Ng, S.H. Seow, M.J.G. Moderscheim, J. Mater. Chem. 2 (1992) 1135.
[13] A.C. Grimsdale, Ph. Leclère, R. Lazzaroni, J.D. MacKenzie, C. Murphy, S. Setayesh, C. Silva, R.H. Friend, K. Müllen, Adv. Funct. Mater. 2 (2002) 729.
[14] M. Surin, P. Sonar, A.C. Grimsdale, K. Müllen, R. Lazzaroni, Ph. Leclère, Adv. Funct. Mater. 15 (2005) 1426.
[15] M. Surin, P. Sonar, A.C. Grimsdale, K. Müllen, S. De Feyter, S. Habuchi, S. Sarzi, E. Braeken, A. Ver Heyen, M. Van der Auweraer, F.C. De Schryver, M. Cavallini, J.F. Moulin, F. Biscarini, C. Femoni, R. Lazzaroni, Ph. Leclère, J. Mater. Chem. 17 (2007) 728.
[16] Ph. Leclère, M. Surin, P. Brocorens, M. Cavallini, F. Biscarini, R. Lazzaroni, Mater. Sci. Eng. Rep. 1 (2006) 55.
[17] Ph. Leclère, E. Hennebieq, A. Calderone, P. Brocorens, A.C. Grimsdale, K. Müllen, J.L. Brèdas, R. Lazzaroni, Prog. Poly. Sci. 28 (2003) 55.